Analysis of complex molecular dynamics in an organic liquid by polarization selective subpicosecond transient grating experiments

F. W. Deeg[a] and M. D. Fayer
Department of Chemistry, Stanford University, Stanford, California 94305

(Received 21 March 1989; accepted 27 April 1989)

We present a subpicosecond time resolved polarization selective transient grating (TG) investigation of pentylcyanobiphenyl (5CB) in its isotropic liquid phase. This system shows complex molecular dynamics with various contributions to the TG signal. With an excitation wavelength $\lambda_{exc} = 665$ nm one induces an anisotropy in the sample from the electronic and nuclear Kerr effects. Exciting with $\lambda_{exc} = 575$ nm generates an excited state grating because of two photon absorption. Solvent relaxation around the excited molecule on a few ps time scale is observed because it spectrally shifts the excited state–excited state transition which is monitored by the TG signal. In addition, radiationless relaxation leads to local heating of the sample in a spatial pattern which mimics the optical interference pattern which established the TG. The heating generates an acoustic standing wave. It is demonstrated that with a single TG setup, polarization selection allows separation and identification of all of the above-mentioned physical processes as they are characterized by different symmetries of the nonlinear susceptibility tensor $\chi^{(3)}$

I. INTRODUCTION

The use of the transient grating (TG) technique in the investigation of physical phenomena has expanded dramatically in recent years.[1–3] The TG approach has been applied to, e.g., the study of thermal energy transport,[4] flow studies in liquids,[5] laser induced ultrasonics,[6] electronic energy transport in solids and liquids,[7] carrier dynamics in semiconductors,[8] Kerr relaxation phenomena,[9] and photochemical reactions.[10] In most of these cases the response of the system has been dominated by one or two easily separable and identifiable physical effects.

In this paper we present a subpicosecond time resolved TG study of an organic liquid, pentylcyanobiphenyl (5CB), which exhibits a complex nonlinear response. We observe (nonresonant) optical field induced electronic and nuclear Kerr effects. The electronic Kerr effect is the essentially instantaneous polarization of the electrons by the applied optical field. The nuclear Kerr effect arises from the small orientational anisotropy induced by the applied field. The time dependence of the nuclear Kerr effect is determined by the molecular reorientational dynamics.[11–13] 5CB forms a liquid crystalline phase. Therefore, even above the phase transition in the isotropic phase studied here, there is considerable local order.[14] The local order is like that found in the nematic phase, but it does not extend over macroscopic distances. Unlike simple liquids, 5CB reorientational relaxation is not hydrodynamic, i.e., it cannot be described in terms of the Stokes–Einstein–Debye model. The nature of the reorientational dynamics probed by the TG nuclear Kerr effect will be discussed in detail in subsequent publications.[15] Here the focus is on the separation of the various contributions to the four wave mixing signal and on the electronic excited state grating contribution to the signal.

Using light with a wavelength $\lambda = 575$ nm an excited state grating is created by two-photon absorption. The electronic ground state of 5CB has a large, permanent electric dipole moment.[16] Upon optical excitation, the dipole moment changes by 5 to 10 Debye.[16] The large change in dipole moment will cause the surrounding molecules to undergo a structural reorganization. The unexcited 5CB molecules can be pictured as a solvent for the excited molecule, and solvent relaxation occurs in a manner analogous to solvent relaxation in dilute solutions of chromophores.[17] Solvent relaxation in dilute solution has recently been investigated by observing ps time resolved changes in fluorescence spectra.[18–20]

In the experiments reported here, solvent relaxation is monitored by probing an excited state–excited state (ES–ES) absorption of 5CB. Initially, the probe wavelength is only slightly absorbed. As the solvent relaxes, the ES–ES spectrum moves onto resonance with the probe wavelength. Therefore, solvent relaxation manifest itself as a time-dependent growth of the TG signal.

Absorptive heating generates acoustic waves in the sample giving rise to typical laser induced phonons (LIPS) signals on a ns time scale. The spatial dependence of the absorptive heating mimics the spatial dependence of the excitation fringe pattern. The fast, spatially periodic heating of the sample launches counter propagating acoustic waves, having a wavelength which matches the fringe spacing. The counter propagating waves combine to give a standing acoustic wave. Thus, there is a spatially periodic, time-dependent oscillation of the sample density. This gives rise to oscilatory diffraction of the probe beam as the time delay between excitation and probe is scanned.[6]

In this paper, we extend an approach of Etchepare *et al.*[21] who recently showed how to separate the electronic and nuclear optical Kerr effect (OKE) in a study of CS_2. We demonstrate how to separate and identify all the above-mentioned physical effects by a careful study of the polarization and intensity dependence of the TG signal.

[a] Permanent address: Institut für Physikalische Chemie, Universität München, Sophienstrasse 11, 8000 Müchen 2, Federal Republic of Germany.

 0021-9606/89/162269-11$02.10

II. EXPERIMENTAL DETAILS

The grating experiments were performed with a subpicosecond dye laser system which is described in detail elsewhere.[22] The dye laser is ultrashort pulse pumped by the fiber-grating compressed and frequency doubled output of a modified Spectra-Physics model 3000 mode-locked continuous wave (cw) Nd:YAG laser. The dye laser generates tunable 200–300 fs pulses, several nJ in energy, at 83 MHz rep rate. These pulses are amplified in a three-stage chain pumped by the frequency doubled output of a cavity dumped Q-switched mode-locked Nd:YAG laser running at a 1 kHz repetition rate. Typical amplifying pulse energies are 700 μJ in the green. A saturable absorber between the second and third amplifier stages suppresses the unamplified dye pulses and shortens the amplified ones. The two Nd:YAG lasers are electronically synchronized by a common radio-frequency (rf) master oscillator for both mode lockers, and the timing is set by a voltage-controlled phase shifter for the rf into the amplifying laser's mode locker. With Rh6G pulse widths in the range 200 to 300 fs and average pulse energies of 40–50 μJ are obtained; for DCM these values are 150 to 250 fs and 10–20 μJ. Amplitude fluctuations of the amplified pulses are minimized with an electronic control system which measures the intensity of the amplified pulses and uses the intensity to feed back and control the phase of the rf into the mode locker of the amplifying laser.[22]

For the OKE TG experiments described here, the amplified pulse is split three ways to yield the two excitation pulses and the probe pulse. The two excitation pulses, focussed to 120 μm spot sizes, are crossed in the sample at an angle of 15° to induce a spatially periodic excitation of the sample (see Fig. 1). The spatially periodic excitation of the sample acts as a Bragg diffraction grating. The time dependence of the grating is monitored by the 90 μm spot size probe pulse which is incident at the phase matching angle for Bragg diffraction (slightly noncollinear with one of the excitation beams to achieve spatial separation of the outgoing signal beam). The probe pulse can be variably delayed by an optical delay line which is controlled by a 1 μm resolution stepper motor. The intensity as well as the polarization of all three beams can be independently controlled by sets of half-wave plates and linear polarizers. A fourth linear polarizer is placed in the signal path and allows any polarization of the diffracted beam to be monitored. Typical pulse energies used in the experiments were in the range 100 nJ–2 μJ for the excitation pulses and 40–100 nJ for the probe pulse. One of the excitation beams or the probe beam is chopped and the signal, which is picked up by a photodiode or a photomultiplier, is fed to a lock-in amplifier. The output of the lock-in amplifier is connected to a computer which allows signal averaging by controlling multiple scans of the optical delay line.

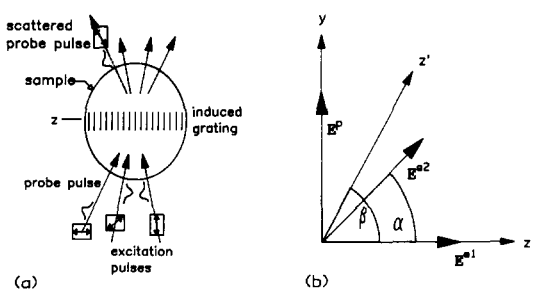

FIG. 1. Schematic illustration of the transient grating experiment. (a) The crossed excitation pulses (optical interference pattern) generate a spatially periodic perturbation of the sample. The resulting changes in the index of refraction create a diffraction grating which Bragg scatters the probe pulse. The polarizations of all four pulses are controlled in the experiment and are used to separate and identify contributions to the signal from various physical processes. (b) Illustration of the polarization configuration used in the experiments. The E fields of the two excitation beams and the probe beam are labeled $e1$, $e2$, and p, respectively. β is the polarization of a polarizer in the signal (diffracted) beam.

III. THEORY

The treatment of a four-wave mixing (FWM) process generally starts with the relationship[23]

$$P_i(\omega) = \chi^{(3)}_{ijkl}(\omega,\omega_3,\omega_2,\omega_1)E_j(\omega_3)E_k(\omega_2)E_l(\omega_1) \tag{1}$$

between the component P_i of the induced polarization in the medium and the components of the electric fields E_j, E_k, and E_l. This relationship is characterized by the properties of $\chi^{(3)}_{ijkl}$, the elements of the third-order nonlinear susceptibility tensor. For the evaluation of a time resolved experiment a description of the FWM process in the time domain

$$P_i(t) = \int_{-\infty}^{+\infty} dt_3 \int_{-\infty}^{+\infty} dt_2 \int_{-\infty}^{+\infty} dt_1 \times \chi^{(3)}_{ijkl}(t-t_3,t-t_2,t-t_1)E_j(t_3) \times E_k(t_2)E_l(t_1) \tag{2}$$

is more convenient. Here $\chi^{(3)}_{ijkl}(t-t_3,t-t_2,t-t_1)$ is the Fourier transform of $\chi^{(3)}_{ijkl}(\omega)$ in Eq. (1). In general one is interested in the *time* dependence of $\chi^{(3)}_{ijkl}(t-t_3,t-t_2,t-t_1)$ because it can provide valuable information about the specific molecular dynamics of the sample under investigation. The *symmetry* properties of the $\chi^{(3)}$ tensor depend on the nature of the observed physical phenomena. Since different physical processes are characterized by different $\chi^{(3)}$ symmetries, polarization-dependent FWM experiments can be used to distinguish and separate time-dependent signals arising from the physical processes. The work described here extends the approach of Etchepare *et al.*[21] who recently showed how to separate the electronic and nuclear contributions to the Kerr effect in CS_2 through a polarization selective TG experiment.

There exist certain relationships among the elements of

Pentylcyanobiphenyl (5CB) from BDH was filtered through a pore size of 0.2 μm to remove dust particles. The liquid was placed inside a sealed 1 mm spectrophotometric cuvette which was inserted into a variable temperature cell. The cell temperature could be regulated and controlled within $\pm$ 0.2 °C. All experiments described here were performed at 42 °C in the isotropic phase of 5CB (nematic–isotropic phase transition temperature T_p = 35 °C).

$\chi^{(3)}$ by virtue of the spatial symmetry class of the material under consideration. These relations have been tabulated by Butcher.[24] For an isotropic sample like a liquid or glass, there are 21 nonzero elements of $\chi^{(3)}$ of which only three are independent. These are $\chi^{(3)}_{1111}$, $\chi^{(3)}_{1122}$ and $\chi^{(3)}_{1212}$ with

$$\chi^{(3)}_{1221} = \chi^{(3)}_{1111} - \chi^{(3)}_{1122} - \chi^{(3)}_{1212}. \tag{3}$$

Hellwarth[25] has shown that the Born–Oppenheimer approximation imposes additional restraints on the symmetry properties of $\chi^{(3)}$. For an isotropic sample the electronic $\chi^{(3)}(e)$ is a scalar and the relationship among the elements of $\chi^{(3)}(e)$ are given by

$$\chi^{(3)}_{1111}(e) = 3\chi^{(3)}_{1122}(e) = 3\chi^{(3)}_{1212}(e) = 3\chi^{(3)}_{1221}(e). \tag{4}$$

$\chi^{(3)}(n)$ which describes all processes associated with nuclear motions contains only the two independent elements $\chi^{(3)}_{1111}(n)$ and $\chi^{(3)}_{1122}(n)$, and the relations

$$\chi^{(3)}_{1221}(n) = \chi^{(3)}_{1212}(n) = [\chi^{(3)}_{1111}(n) - \chi^{(3)}_{1122}(n)]/2. \tag{5}$$

With these general relationships due to the space symmetry group and the Born–Oppenheimer approximation, let us now consider the special symmetry properties of $\chi^{(3)}$ which arise from the symmetry of the underlying physical mechanism which generates $\chi^{(3)}$.

The optical Kerr effect (OKE) has two contributions. The first is the electronic OKE which is caused by the virtually instantaneous distortion of the molecular electron cloud by the applied optical field. The second is the nuclear OKE which comes about by the slower reorientation of the nuclei in the optical field. The properties of $\chi^{(3)}$ (e OKE) for the electronic OKE are given by the relationships in Eq. (4). It can be shown[15] for the nuclear OKE, that

$$\chi^{(3)}_{1111}(n\,\mathrm{OKE}) = a + b, \tag{6a}$$

$$\chi^{(3)}_{1122}(n\,\mathrm{OKE}) = a, \tag{6b}$$

and with Eq. (5),

$$\chi^{(3)}_{1212}(n\,\mathrm{OKE}) = b/2. \tag{6c}$$

a and b are often referred to as the "isotropic" and "anisotropic" parts of the susceptibility[26] as they are the quantities which are responsible for polarized and depolarized scattered light, respectively. For liquids, theories which relate the third-order nonlinear susceptibility $\chi^{(3)}$ to the linear molecular polarizability α, have shown the equation

$$b \approx -3a \tag{7}$$

should hold.[25] In general, this has been confirmed by experiments. The experimental approach described in this paper provides a straightforward method to test relation (7). Inserting Eq. (7) into Eqs. (6) gives

$$\chi^{(3)}_{1111}(n\,\mathrm{OKE}) = -2\chi^{(3)}_{1122}(n\,\mathrm{OKE}) = (4/3)\chi^{(3)}_{1212}(n\,\mathrm{OKE}). \tag{8}$$

We now turn to electronic excited state contributions to $\chi^{(3)}$. Myers and Hochstrasser[27] have recently compared different experimental methods which use absorption for the study of orientational relaxation. Within the general theoretical framework of FWM they find

$$\chi^{(3)}_{1111}(\mathrm{ex}) = (1/3)(1 + 2r), \tag{9a}$$

$$\chi^{(3)}_{1122}(\mathrm{ex}) = (1/3)(1 - r), \tag{9b}$$

and

$$\chi^{(3)}_{1212}(\mathrm{ex}) = r/2 \tag{9c}$$

with the anisotropy r defined by

$$r = (2/5)\langle P_2[\boldsymbol{\mu}_i \cdot \boldsymbol{\mu}_j]\rangle = (1/5)\langle 3\cos^2(\boldsymbol{\mu}_i \cdot \boldsymbol{\mu}_j) - 1\rangle. \tag{10}$$

$\boldsymbol{\mu}_i$ and $\boldsymbol{\mu}_j$ are the transition dipole moments of the transition which is excited and the transition which is probed, respectively. These need not be the same. P_2 is the second Legendre polynomial, and the brackets in Eq. (10) stand for angular average.

We want to discuss several special cases for the relationship between $\boldsymbol{\mu}_i$ and $\boldsymbol{\mu}_j$ and the corresponding $\chi^{(3)}$ tensor. If $\boldsymbol{\mu}_i$ and $\boldsymbol{\mu}_j$ are parallel to each other, $r = 2/5$ with Eq. (9), and we find with Eq. (10),

$$\chi^{(3)}_{1111}(\|\mathrm{ex}) = 3\chi^{(3)}_{1122}(\|\mathrm{ex}) = 3\chi^{(3)}_{1212}(\|\mathrm{ex}). \tag{11}$$

If $\boldsymbol{\mu}_i$ and $\boldsymbol{\mu}_j$ are perpendicular to each other, $r = -1/5$, and

$$\chi^{(3)}_{1111}(\perp\mathrm{ex}) = (1/2)\chi^{(3)}_{1122}(\perp\mathrm{ex}) = -2\chi^{(3)}_{1212}(\perp\mathrm{ex}). \tag{12}$$

If there is no correlation between $\boldsymbol{\mu}_i$ and $\boldsymbol{\mu}_j$, $r = 0$ and

$$\chi^{(3)}_{1111}(\phi\mathrm{ex}) = \chi^{(3)}_{1122}(\phi\mathrm{ex}) \tag{13a}$$

and

$$\chi^{(3)}_{1212}(\phi\mathrm{ex}) = 0. \tag{13b}$$

Turning now to acoustic phenomena, there are two mechanisms for the optical generation of acoustic waves.[2,6] The first is local heating in the sample due to optical absorption and radiationless relaxation. The second is direct electrostrictive coupling of the optical pulses and the acoustic field of the sample. In isotropic samples both mechanisms (although distinguishable by their time dependence) have the same symmetry properties. In addition, a nonpropagating thermal contribution to $\chi^{(3)}$ also has the same symmetry properties. Acoustic waves and a thermal disturbance induce an isotropic local density change characterized by

$$\chi^{(3)}_{1111}(\mathrm{ac}) = \chi^{(3)}_{1122}(\mathrm{ac}) \tag{14a}$$

and

$$\chi^{(3)}_{1212}(\mathrm{ac}) = 0. \tag{14b}$$

The relations (4)–(14) give the constraints that various physical processes impose on the symmetry of $\chi^{(3)}$. We have explicitly considered six different physical situations: Electronic and nuclear OKE, excited state population characterized by parallel, perpendicular, and uncorrelated transition dipole moments and acoustic waves (thermal disturbance). Acoustic waves and "uncorrelated" excited state population result in the same symmetry constraints on $\chi^{(3)}$. "Parallel" excited state population and the electronic OKE have the same symmetry properties. In general, however, different physical processes are described by different $\chi^{(3)}$ symmetries.

We now want to investigate the implictions of these symmetry relations on different TG experimental configurations.

The schematics of the TG experiment in Fig. 1 show the two excitation beams and the probe beam striking the sample and the generated signal beam. The polarizations i, j, k, and l of the four pulses, which are controlled by polarizers in the beam paths, determine the elements of $\chi^{(3)}$ which are observed.

In an ordinary grating experiment, the two excitation beams have the same polarization. Let us assume they are polarized in the scattering plane (in our convention along the z axis). If we choose the same z polarization for the probe beam and the measured signal beam,

$$P = \chi^{(3)}_{1111} E^p E^{e1} E^{e2}. \tag{15}$$

Here the superscript stands for the probe beam p and the two excitation beams $e1$ and $e2$. While discussing the symmetry properties of the experiment, we will omit the time dependence of the quantities in Eq. (15). If we use a perpendicular y polarization for probe pulse and detect the signal pulse through a y oriented polarizer, the observed signal becomes

$$P = \chi^{(3)}_{1122} E^p E^{e1} E^{e2}. \tag{16}$$

Examining Eqs. (4)–(14), it can be seen that all phenomena discussed contribute to the parallel as well as the perpendicular probed ordinary grating, although different phenomena contribute to varying degrees. This configuration does not allow us to suppress or single out a particular physical process.

In a crossed grating the two excitation beams have perpendicular polarization. If we now bring in the probe pulse with z polarization and measure the perpendicular y polarized signal we obtain

$$P = \chi^{(3)}_{1212} E^p E^{e1} E^{e2}. \tag{17}$$

The Eqs. (13) and (14) show that acoustic waves and the "uncorrelated" excited state grating do *not* generate a signal in this configuration and that a discrimination with respect to these contributions is possible. The crossed grating has been applied to the separation of Kerr effect and acoustic waves earlier.[9]

In a generalization of this polarization selective approach, the two excitation beams have polarizations which differ by an angle unequal to 0° or 90°. Let us assume the polarization of one excitation beam is z and the polarization of the other excitation beam is at an angle α with respect to z, as shown in Fig. 1(b). Under these circumstances a y-polarized probe pulse induces sample polarizations P_z and P_y (and associated signal strengths) along the z and y axes which are given by

$$P_z = \chi^{(3)}_{1212} \sin\alpha E^p E^{e1} E^{e2} \tag{18a}$$

and

$$P_y = \chi^{(3)}_{1122} \cos\alpha E^p E^{e1} E^{e2}. \tag{18b}$$

From Eqs. (18) we can calculate the polarization along z' which is at an angle β with respect to the z axis [see Fig. 1(b)] as

$$\begin{aligned} P_{z'} &= P_y \sin\beta + P_z \cos\beta \\ &= (\chi^{(3)}_{1122} \cos\alpha \sin\beta + \chi^{(3)}_{1212} \sin\alpha \cos\beta) \\ &\quad \times E^p E^{e1} E^{e2}. \end{aligned} \tag{19}$$

This general polarization selective TG configuration allows one to suppress the signal contribution of any process which is characterized by a specific $\chi^{(3)}$ symmetry.

To be specific, let us choose $\alpha = 45°$ to obtain from Eq. (19),

$$P_{z'} = (\chi^{(3)}_{1122} \sin\beta + \chi^{(3)}_{1212} \cos\beta) E^p E^{e1} E^{e2}. \tag{20}$$

With Eq. (20) we can calculate the angle β_0 for the signal polarization which makes a certain contribution to the signal disappear, i.e.,

$$\beta_0 = \tan^{-1}(-\chi^{(3)}_{1212}/\chi^{(3)}_{1122}). \tag{21}$$

For the electronic OKE, using, e.g., Eq. (4) one obtains $\beta_0 = 135°$. We will use the notation (0°/45°/90°/135°) for this configuration which suppresses the electronic OKE contribution to the signal. In the notation the four quantities within parentheses stand for the angles of polarization of the two excitation beams, the probe beam and the signal beam in that order. For all processes considered in this paper, Table I lists the angle β_0 in a (0°/45°/90°/β_0) polarization configuration which suppresses the response of the given physical mechanism.

For the interpretation of the signals recorded in the TG experiments described here, it is also necessary to consider the explicit *time* dependence. If we assume that the two excitation pulses are time coincident at the sample at $t' = t_1 = t_2$ and that we can separate excitation and probe processes, $\chi^{(3)}_{ijkl}(t - t_3) = \delta(t - t_3)$, Eq. (2) gives

$$\begin{aligned} P_i(t) &= E^p_j(t) \int_{-\infty}^{t} dt' \chi^{(3)}_{ijkl}(t - t') \\ &\quad \times E^{e1}_k(t') E^{e2}_l(t'). \end{aligned} \tag{22}$$

To calculate the Bragg scattered energy $U(\tau)$ of a probe pulse delayed by τ with respect to the excitation pulses, it is necessary to perform the convolution with the probe pulse to obtain

TABLE I. Signal beam polarization angle β_0 which suppresses the contribution of the given physical process to the transient grating signal from an isotropic liquid. The polarizations of the four beams are (0°/45°/90°/β); see the text.

Physical mechanism	β_0
Electronic OKE	135°
Nuclear OKE	56.3°
Excited state grating:	
(a) general case, $r = r_0$	$\tan^{-1}[-1.5r_0/(1 - r_0)]$
(b) $\mu_i \parallel \mu_j$, $r = 2/5$	135°
(c) $\mu_i \perp \mu_j$, $r = -1/5$	14.0°
(d) μ_i and μ_j uncorrelated, $r = 0$	0°
Acoustic wave (or thermal perturbation)	0°

$$U_i(\tau) = \int_{-\infty}^{+\infty} dt\, I_j^p(\tau - t) \times \left[\int_{-\infty}^{t} dt'\, \chi_{ijkl}^{(3)}(t-t') I_{kl}^e(t')\right]^2. \quad (23)$$

In Eq. (23) the light intensities I of the pulses are used instead of the electric field amplitudes E and the two excitation pulses have the same intensities. In Eq. (23), the second integral represents the convolution of the system response with the excitation pulses. The first integral is the additional convolution with the probe pulse.

IV. RESULTS AND DISCUSSION

Complex liquids can display a wide variety of dynamical phenomena. Here the emphasis is on isolating and identifying the various contributions to the TG signals which arise from 5CB. Of particular interest is the fast time scale reorientational dynamics of 5CB in the pretransitional isotropic phase. The reorientational dynamics can be examined using TG observations of the nuclear OKE. The detailed results of this investigation will be published elsewhere.[15]

To separate the electronic and nuclear OKE, the polarization selective approach described in Sec. III was employed. Figure 2 shows the time dependence of the recorded TG signals exciting (and probing) with $\lambda_{ex} = 575$ nm and with excitation pulse energies $U_{ex} = 1\ \mu$J. The curves show the signal for different angles β of the signal polarization in a (0°/45°/90°/β) configuration. The drastic changes of the shape of the signal demonstrate that processes with a variety of $\chi^{(3)}$ symmetries contribute to the signal. There exist (at least) two contributions: a nearly symmetric spike at times $\tau < 1$ ps and a much slower process with a rise time of 4 ps and a decay on a 100 ps time scale. As shown in Table I, the electronic OKE signal should vanish for $\beta = 135°$. Consulting Fig. 2, we see that the spike-like feature at $\tau = 0$, which is dominant for $\beta = 0°$, does indeed get smaller with increasing β and goes through a minimum for $\beta = 135°$. This feature is the electronic OKE. It time dependence is the instrument response since the electronic OKE relaxes fast (10^{-15} s) compared to the pulse widths in the experiment. The fact that the electronic OKE signal cannot be extinguished completely is due to its large amplitude and a small depolarization in the sample cell.

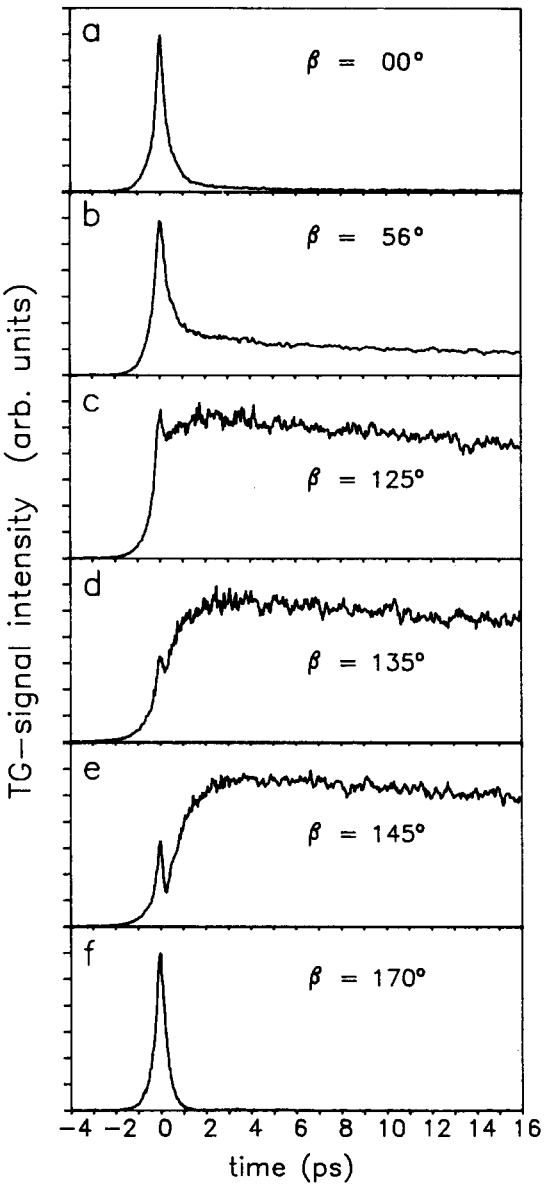

FIG. 2. Fast time scale time dependence of TG signals for an excitation wavelength $\lambda_{ex} = 575$ nm and excitation pulse energies $U_{ex} = 1\ \mu$J. All signals are recorded in a (0°/45°/90°/β) polarization configuration with β as indicated. The vertical scales are chosen to give all signals the same maximum amplitude. As the detection polarization, β, is changed, the characteristics of the signal change dramatically.

It is interesting to note the difference between Figs. 2(c) and 2(e). These figures present data taken with experimental configurations for which the contributions of the electronic OKE to the TG signal should be of comparable magnitudes. However, these contributions have opposite signs. In one case [Fig. 2(c)], the polarization due to the electronic OKE has the same sign as the polarization of the slowly varying process; in the other case [Fig. 2(e)] it has the opposite sign. The TG signal is essentially proportional to the square of the nonlinear susceptibility $\chi^{(3)}$ [see Eq. (23)]. Therefore, in Fig. 2(c) the electronic OKE appears as a peak in the signal, while in Fig. 2(e) it appears as a dip in the signal. Because of the imperfect time resolution of the experiment the signal in Fig. 2(e) does not return to 0 after the first maximum.

The nuclear OKE is expected to vanish for $\beta = 56°$ as indicated in Table I. As shown in Fig. 2(b), however, the slowly varying process can be easily detected for $\beta = 56°$ and actually disappears for $\beta = 170°$ [(Fig. 2(e)]. This strongly suggests that the observed grating is not caused by a nuclear OKE but rather arises from a different physical phenomenon. Figure 3 shows an excitation pulse energy dependence of the TG signal for $\beta = 100°$, a polarization configuration in which both effects contribute appreciably to the signal. For a set spotsize and pulsewidth the light intensity I is proportional to the pulse energy. As pulse energies can be readily measured we will consistently use pulse energies in discussions of intensity effects. Comparing the data for the three excitation energies, U_{ex}, shown in Figs. 3(a)–3(c), it is clear that the slow process exhibits a different and steeper intensity dependence than the electronic OKE.

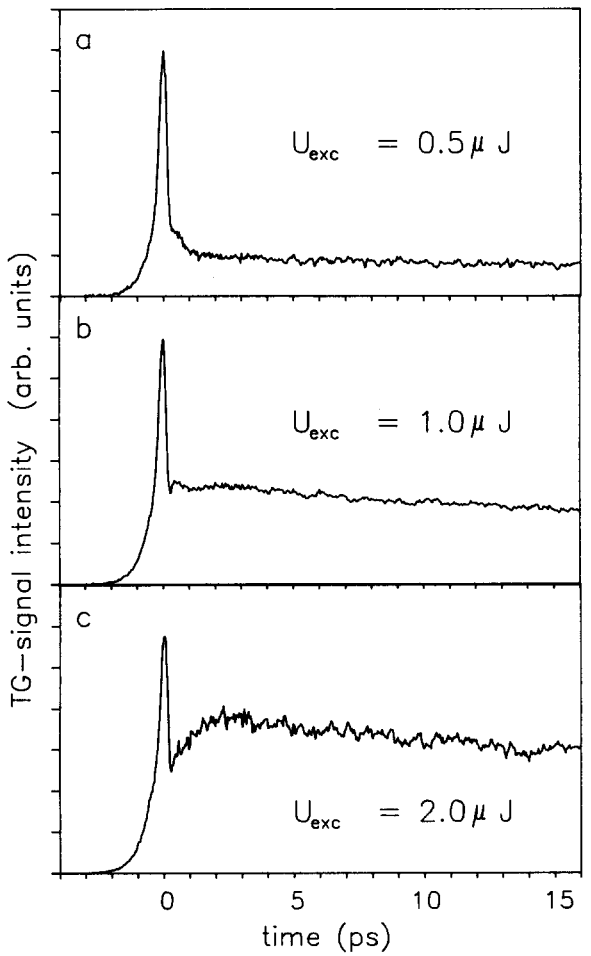

FIG. 3. Fast time scale time dependence of TG signals for an excitation wavelength $\lambda_{ex} = 575$ nm and a (0°/45°/90°/100°) polarization configuration. As indicated the excitation pulse energy changes by a factor of 2 from (a) to (b) and (b) to (c). The vertical scales are chosen to give all signals the same maximum amplitude. The change of the signal shape demonstrates the different intensity dependences of the electronic OKE and the excited state grating.

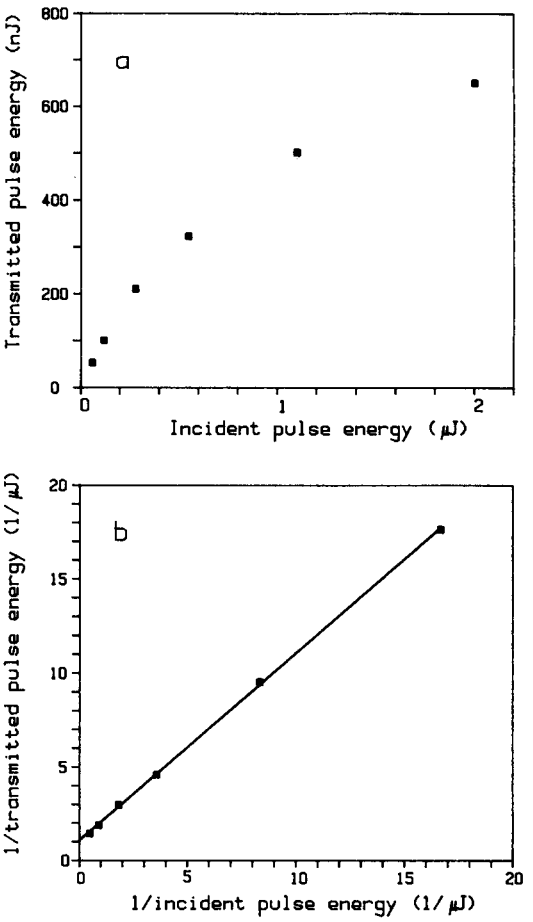

FIG. 4. Absorption of 300 fs light pulses with $\lambda = 575$ nm and pulse energies as indicated in a 1 mm thick sample of 5CB. (a) Transmitted pulse energies vs incident pulse energies. The data points demonstrate the nonlinear absorption in the sample. (b) Plot of incident and transmitted pulse energies according to Eq. (24b). The straight line through the data points represents a linear fit as expected for a two-photon absorption.

The steep intensity dependence for the slow component suggests the generation of an electronic excited state grating by two-photon absorption. Strong two-photon absorption for $\lambda_{ex} = 575$ nm is not surprising if one consults the one-photon spectra of cyanobiphenyl (OCB) and octylcyanobiphenyl (8CB) shown by David and Baeyens-Volant.[19] These show a strong lowest energy absorption band centered at $\lambda_{abs} = 262$–281 nm, depending on the solvent polarity. Because of the low symmetry of the CB molecules (C_2) all one-photon transitions should be two-photon allowed and vice versa, and the two-photon spectrum should essentially follow the one-photon spectrum. Therefore, with $\lambda_{ex} = 575$ nm one would expect to two-photon excite into the red edge of the lowest-lying absorption band and populate the lowest excited singlet state S_1.

To investigate the magnitude of two-photon absorption in the sample at the excitation wavelength $\lambda_{ex} = 575$ nm, a simple single beam absorption experiment, measuring the incident and transmitted energy for various light intensities, was performed. The results are shown in Fig. 4. A plot of the transmitted light energy U_{trans} vs the incident light energy U_{in} shows the typical two-photon behavior[23]

$$U_{trans} = \frac{U_{in}}{1 + \gamma\omega z_0 U_{in}} \tag{24a}$$

or

$$1/U_{trans} = 1/U_{in} + \gamma\omega z_0. \tag{24b}$$

Here z_0 is the sample thickness, ω is the frequency of the light and γ the two-photon (energy) absorption coefficient. From a linear fit to the data plotted in Fig. 4(b) one obtains $\gamma\omega z_0 = 11 \pm 1\,\mu J^{-1}$ and $\gamma = (3.4 \pm 0.4)\ 10^{-9}$ Js/cm. The two-photon absorption is corroborated by the blue fluorescent light emitted from the sample upon excitation with moderate to intense light pulses of $\lambda_{ex} = 575$ nm.

Returning to Fig. 4(b) and comparing that plot with the typical excitation energies used to generate the signals in Fig. 3, one realizes that the experiments are conducted with intensities at which a considerable amount of the incident light is absorbed in the sample. Moreover, the light intensity in the peaks of the optical interference pattern is 4 times as high as in a single excitation beam, further enhancing the nonlinear absorption. Because of beam depletion the excitation energy

dependence of the excited state grating in Fig. 3 is not $\propto (U^2)^2$ [the second square comes from the grating or FWM configuration, see Eqs. (23)] and the dependence of the electronic OKE signal is not $\propto U^2$. Because of the large nonlinear absorption in the sample, the dependence of the signal on the excitation energy is shallower than expected. In the limit of negligible absorption, $\gamma\omega z_0 U_{\text{in}} \ll 1$, one can expect the theoretical U dependence to be observed. For decreasing excitation energies, we find the electronic OKE and the excited state TG signal asymptotically approach a U^2 an U^4 dependence. For $U_{\text{exc}} < 100$ nJ the electronic OKE obeys a U^2 law.

The time dependence of the excited state TG signal [see Fig. 2(d)] is characterized by a rise time of 4 ps. To understand the origin of this rise time, it is neccassary to know the characteristics of the probing process. A change of the probe pulse energy U_p shows that the signal is linear in the probe pulse intensity. This is expected for an one-photon process [see Eq. (23)]. Since the sample does not absorb at $\lambda_p = 575$ nm, the probe pulse must be absorbed by an excited state–excited state transition. Thus, the intensity of the diffracted signal depends on a probe absorption from S_1 to some higher lying excited state S_n. If a high-lying vibration of S_1 were initially populated, vibrational relaxation to the bottom of the S_1 manifold could result in increased probe absorption and the rise in the signal. However, as mentioned earlier, the two-photon excitation reaches only the red edge of the lowest-lying absorption band and does not generate any vibrationally excited states of S_1.

A careful study of the absorption and fluorescence spectra of OCB and 8CB in a series of solvents with different polarity[16] points to the explanation. The fluorescence spectra are characterized by a strong red shift of the emission with increasing solvent polarity. These spectral shifts are due to a change of the permanent dipole moment of the CB molecules upon excitation into S_1. The change in the dipole moment is very large, on the order of 5–10 D. Because of this large dipole moment change upon excitation, there will be extensive rearrangement of the "solvent cage" (cage of unexcited 5CB molecules). The unexcited 5CB molecules move under the influence of the new electric field produced by the change in dipole moment of the excited molecule.[17–20]

The known spectroscopy of the class of molecules of which 5CB is a member strongly suggests that solvent relaxation is observed in the excited state TG signal. This behavior is illustrated in Fig. 5. Two photons excite the molecule from S_0 to S_1. The probe wavelength lies within the region of the S_1 to S_2 absorption. The transition probability from S_1 to S_2 is small for a photon with $\lambda_p = 575$ nm, and the TG signal is initially small. Because of the solvent cage reorganization, all state energies change from the unprimed to the primed values (see Fig. 5). A strong $S_1' \to S_2'$ transition is shifted onto the probe beam wavelength, giving rise to a strong TG signal. After the rise of the excited state TG signal which tracks the solvent relaxation, the signal decays because of radiative and radiationless relaxation of the S_1' state to the S_0' state.

Examining the polarization dependence of the excited state TG signal (Fig. 2), we can obtain information about

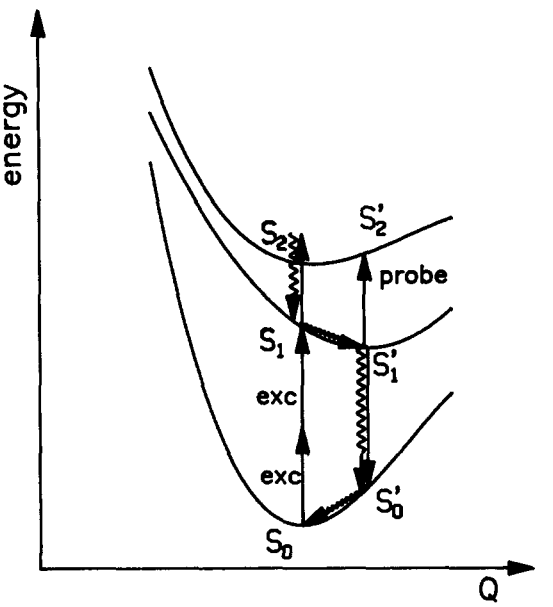

FIG. 5. Schematic diagram of the sequence of steps leading to an excited state and an acoustic wave transient grating signal. At moderate intensities, two photons excite the S_1 state. Solvent reorganization shifts the probe wavelength onto a strong absorption giving a signal that increases at short time [see Fig. 2(d)]. Q is a cooperative nuclear coordinate representing the solvent cage reorganization. At high intensities, a third photon is absorbed during the excitation process. Rapid radiationless relaxation deposits heat and launches an acoustic standing wave [see Fig. 6(c) and 6(d)].

the transition dipole moments involved in the excitation and probe processes. As Fig. 2(f) shows, the excited state TG signal disappears for a (0°/45°/90°/170°) polarization configuration. With Table I $\beta_0 = 170°$ can be used to calculate the anisotropy of the excited state grating $r_0 = 0.105$. Inserting this value into Eq. (10) one obtains $\langle \cos^2(\boldsymbol{\mu}_i \cdot \boldsymbol{\mu}_j) \rangle = 0.51$. Assuming a well-defined relationship between $\boldsymbol{\mu}_i$ and $\boldsymbol{\mu}_j$ for all molecules this corresponds to an angle $\gamma_0 = 45°$ between $\boldsymbol{\mu}_i$ and $\boldsymbol{\mu}_j$. The $S_0 \to S_1$ transition in the CB molecules is polarized along the long axis of the molecule (z), whereas the $S_0 \to S_2$ transition is polarized perpendicular (x or y).[16] Assuming C_2 symmetry, this means that the $S_0 \to S_1$ transition is two-photon xy polarized and the $S_1 \to S_2$ transition is one-photon x or y polarized. These polarization assignments are consistent with the $(\boldsymbol{\mu}_i \cdot \boldsymbol{\mu}_j)$ angle $\gamma_0 = 45°$ and are therefore in accord with the polarization selective TG data.

So far we have discussed the behavior of the TG signal on a time scale of zero to tens of ps. Figure 6 shows the results of the polarization selective TG experiment on a much longer ns time scale. Pronounced oscillations in the TG signal are observed. These are characteristic of acoustic waves generated in a LIPS experiment.[6] A survey of the data in Fig. 6 demonstrates that the LIPS signal disappears for $\beta = 0°$ (or 180°) as predicted by theory (see Table I). It is important to compare Figs. 6(a) and 6(b). The signal polarization β changes only by 10° from a to b, but the two signals convincingly demonstrate the different $\chi^{(3)}$ symmetries of the excited state and the acoustic wave gratings. For $\beta = 170°$, which makes the excited state contribution vanish, there is a strong LIPS signal (and a contribution at $t = 0$ from the electronic

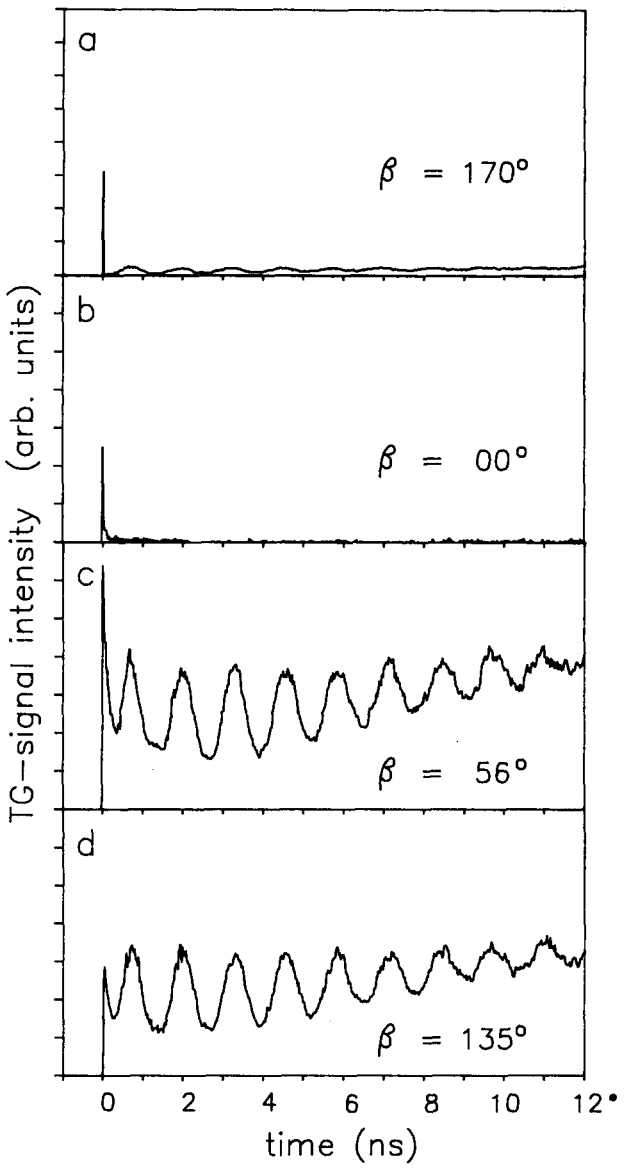

FIG. 6. Slow time scale time dependence of TG signals for an excitation wavelength $\lambda_{ex} = 575$ nm and excitation pulse energies $U_{ex} = 650$ nJ. All signals are recorded in a (0°/45°/90°/β) polarization configuration with β as indicated. The vertical scales are the same in (a)–(d) allowing a direct comparison of the absolute signal amplitudes. The oscillations in the signal are caused by an acoustic standing wave generated by heat deposition from three photon absorption and radiationless relaxation.

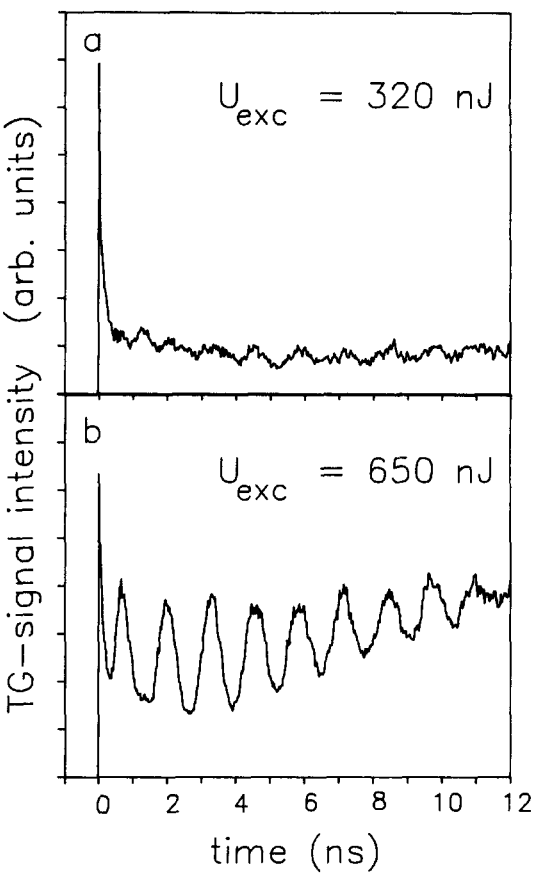

FIG. 7. Slow time scale time dependence of TG signals for an excitation wavelength $\lambda_{ex} = 575$ nm and a (0°/45°/90°/56°) polarization configuration. As indicated the excitation pulse energy changes by a factor of 2 from (a) to (b). The vertical scales are chosen to give the signals the same maximum amplitude. The change of the signal demonstrates the different intensity dependences of the excited state and the acoustic wave grating.

OKE), while for $\beta = 180°$ the acoustic wave contribution is suppressed and the excited state grating is clearly visible.

Figure 7 shows slow time scale signals for two different excitation energies U_{ex}. The two signals are scaled to equal maximum amplitudes. Comparing the contributions of the excited state grating (at $\tau < 200$ ps) and the LIPS oscillations in Figs. 7(a) and 7(b), one finds that the relative amplitude change for the LIPS signal is much larger than for the excited state TG signal. Since the excited state grating is generated by two-photon absorption, we must conclude that (at least) three photons are necessary to induce the large LIPS oscillations. This behavior can be understood in a straightforward manner and is illustrated in Fig. 5. As mentioned earlier, with $\lambda_{ex} = 575$ nm the two photons excite the red edge of the $S_0 \rightarrow S_1$ transition. There is no vibrational relaxation in the S_1 manifold which could deposit heat into the sample and launch an acoustic wave. A third photon during the excitation pulse, however, takes the molecule from S_1 to a higher excited state, and subsequent fast vibrational radiationless relaxation deposits heat into the sample. In this process, the entire energy of the third photon is transformed into heat which generates a large acoustic wave.

The signal in Fig. 7(a) for the lower excitation energy shows an appreciable TG signal on the ns time scale in addition to the low amplitude LIPS oscillations. This indicates that there is another process contributing to the TG signal on this slow time scale. There are two possible explanations. Radiationless relaxation from S_1 to S_0 also releases heat into the sample. The lifetime of S_1 is relatively short [< 1 ns (Ref. 16)] but comparable to the frequency of the acoustic wave. Under these conditions the heat deposition generates predominantly a thermal grating with very small or zero amplitude acoustic waves.[28] The thermal grating will decay on a μs time scale by thermal diffusion. An alternative explanation is intersystem crossing from S_1 to the triplet state T_1. The probe would have to detect the triplet state grating through triplet–triplet absorption. If the transition dipole for this triplet–triplet absorption is uncorrelated with the

original $S_0 \rightarrow S_1$ transition dipole, it can be seen from Table I that the $\chi^{(3)}$ symmetry of this triplet state grating is the same as the symmetry of the acoustic wave grating. That is the corresponding TG signal should disappear for $\beta = 0°$ as found in the experiment [see Fig. 6(b)]. While the experiments presented cannot distinguish between the two possibilities, the thermal grating is perhaps more plausible. There will be some radiationless relaxation which can generate the thermal grating. For the signal to be from a triplet grating, there must be significant intersystem crossing, the probe wavelength must fall on a triplet–triplet absorption, and the triplet–triplet absorption transition dipole direction must have no correlation with the $S_0 \rightarrow S_1$ transition dipole direction. The likelihood of this seems remote.

As is clear from the data presented so far, the TG signals for an excitation wavelength $\lambda_{ex} = 575$ nm are dominated by the two-photon resonance of the 5CB molecules and absorption induced effects. The spectrum of the CB molecules[16] suggests that these resonant effects should disappear if the excitation wavelength is shifted to the red. In Fig. 8 polarization selective TG data with an excitation and probe wavelength of 665 nm are presented. A comparison of Figs. 8 and 2 shows that both polarization and time depedence of the observed signals are very different. In Fig. 8 there are two contributions to the TG signal with different $\chi^{(3)}$ symmetries. In contrast to Fig. 2, the two contributions to the signals in Fig. 8 have comparable time scales. The vertical lines at $\tau = 0$ in Fig. 8 have been added to help visualize the small time shifts of the signal as a function of β. One finds again a TG signal due to the electronic OKE which disappears for $\beta = 135°$. The second contribution, which dominates the signal for $\tau > 1$ or 2 ps, is suppressed for a signal polarization $\beta = 56°$, as predicted by theory for the nuclear OKE.

It is illustrative to compare Figs. 8(c) and 8(e). In these two figures the relative amplitude of nuclear and electronic OKE are comparable. In Fig. 8(e) the induced polarizations have the same sign, while in Fig. 8(c) they have opposite signs. The data in Fig. 8(d) are for a (0°/45°/90°/135°) polarization configuration and an excitation wavelength $\lambda_{ex} = 665$ nm. The electronic OKE signal is absent. Because of the wavelength, there is no two-photon absorption generated excited state grating. The signal displays only the time dependence of the nuclear OKE, and therefore it is possible to study the reorientational dynamics of the 5CB molecules on all time scales.[15] 5CB displays very novel reorientational dynamics on the time scale of a few hundred fs to 200 ps. A recent study using these techniques was conducted on a similar but simpler molecule, biphenyl.[29] The results of detailed temperature studies show that biphenyl behaves "hydrodynamically" following an initial period of librational relaxation. That is on times longer than two ps, orientational diffusion about the long and short axes of the molecule was accurately described by the Stokes–Einstein–Debye equation. The decays at all temperatures are pure biexponentials. In contrast, 5CB yields highly nonexponential decays with decay rates that change by orders of magnitude as the decay is observed over several decades. In addition the nonexponential decay is virtually temperature independent from just above the nematic phase transition to 50° above the phase

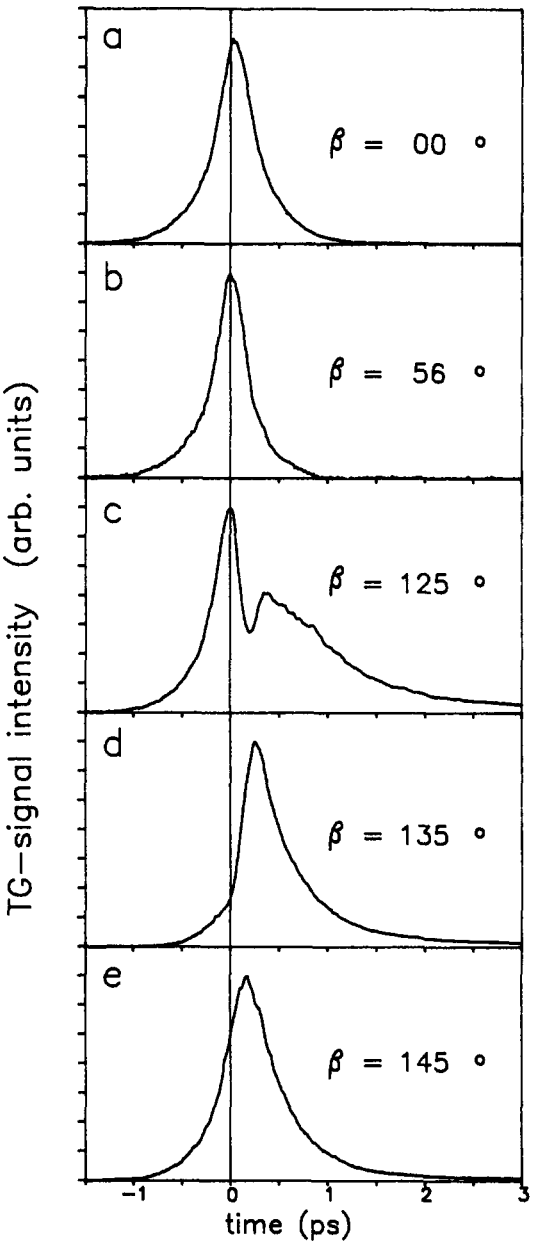

FIG. 8. Fast time scale time dependence of TG signals for an excitation wavelength $\lambda_{ex} = 665$ nm and excitation pulse energies $U_{exc} = 1$ μJ. All signals are recorded in a (0°/45°/90°/β) polarization configuration with β as indicated. The vertical scales are chosen to give the signals the same maximum amplitude. The data in (b) is pure electronic OKE while the data in (d) is pure nuclear OKE. The vertical line at $\tau = 0$ has been added as a visual aid to allow an easier comparison of TG data at different β.

transition. The complete results of the 5CB experiments will be presented and discussed in terms of a model involving the high degree of local structure which exists in the isotropic phase of a liquid crystal.[15]

To illustrate the different $\chi^{(3)}$ symmetries of various physical processes and the isolation of the signals arising from the physical processes through polarization selective TG experiments from a different perspective, Fig. 9 shows the β dependence of the TG signal. The curves display data for a given excitation wavelength and a *fixed* delay τ of the probe pulse with respect to the excitation pulses. The data in Figs. 9(a)–9(c) were recorded with an excitation wave-

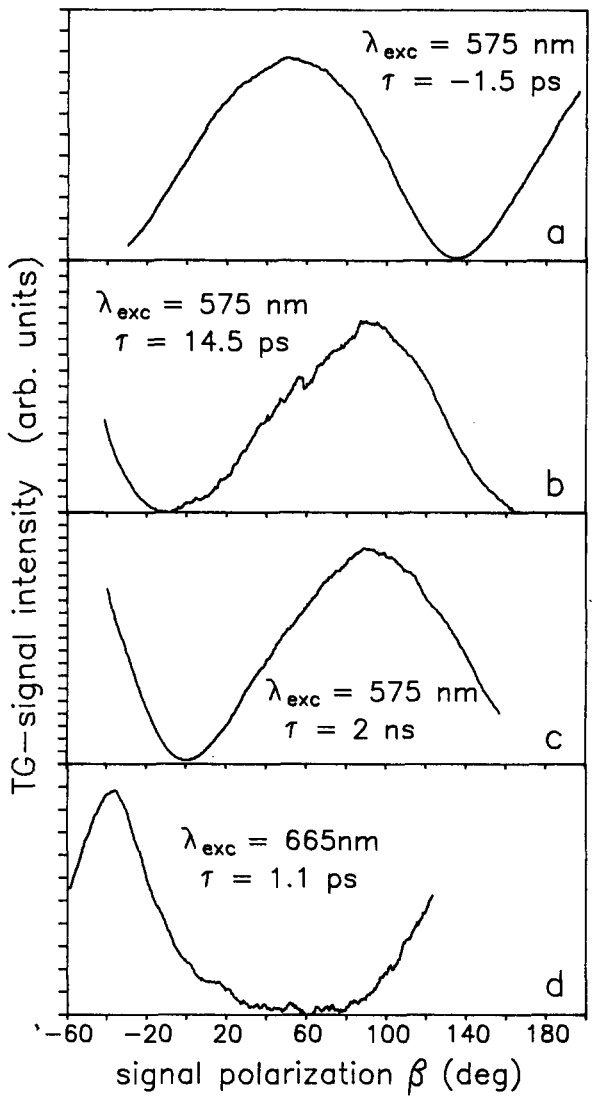

FIG. 9. Dependence of the TG signal intensity on the signal polarization angle β for different excitation wavelengths λ_{ex} and various delays τ of the probe pulse with respect to the excitation pulses. The different β dependences in (a)–(d) illustrate the different $\chi^{(3)}$ symmetries of the various processes monitored under the indicated conditions. (a) Electronic OKE, (b) excited state grating due to two-photon absorption probed by excited state–excited state absorption, (c) acoustic wave grating, (d) nuclear OKE.

length $\lambda_{ex} = 575$ nm, while $\lambda_{ex} = 665$ nm was used to obtain the data in Fig. 9(d). Figure 9(a) shows the polarization dependence of the TG signal when the probe pulse arrives coincident with the leading edge of the excitation pulses. Under these circumstances only the electronic OKE contributes to the signal, and a minimum is observed at $\beta = 135°$. With a fixed probe pulse delay of 14.5 ps [Fig. 9(b)], diffraction is caused by the excited state grating which exhibits a minimum at $\beta = 170°$ (or $-10°$). The graph in Fig. 9(c), for a probe pulse delay $\tau = 2$ ns, records the polarization characteristics of the isotropic acoustic wave grating which disappears for $\beta = 0°$. The signal in Fig. 9(d) has a minimum at approximately $\beta = 60°$, as expected for the nuclear OKE.

All the data shown in this paper have been recorded with a $(0°/45°/90°/\beta)$ polarization configuration. It is important to emphasize that there is nothing unique about this configuration. The same kind of experiments can be performed with any configuration which measures a sample polarization with contributions from two different nonzero elements of the $\chi^{(3)}$ tensor [see Eq. (19)]. Etchepare *et al.* in their OKE investigation of CS_2, for example, have applied a $(0°/0°/45°/\beta)$ configuration.[21] In contrast, a $(0°/90°/\alpha/\beta)$ setup, i.e., a crossed grating or polarization grating, does not work as one measures only $\chi^{(3)}_{1212}$. The fact that there are a variety of configurations which will work allows us to tailor the configuration with other considerations, like S/N ratio, in mind. In the experiments presented here, the main noise source is scattered light from the excitation beam which is nearly collinear with the signal beam. This excitation beam is 45° polarized, and scattered light from it is blocked if the polarizer in the signal path is set at 135°. Thus for $\lambda_{exc} = 665$ nm, the configuration which suppresses the electronic OKE and only records the nuclear OKE also provides the best S/N ratio. Therefore, in general it is possible to choose a polarization configuration which either optimizes the S/N ratio for the specific physical process of interest or which makes the β_0 of two processes one wants to separate as different as possible.

V. CONCLUDING REMARKS

We have described a subpicosecond time resolved polarization selective TG investigation of a neat liquid pentylcyanobiphenyl sample. With nonresonant excitation at a wavelength $\lambda_{exc} = 665$ nm one observes a TG signal which tracks the electronic and nuclear OKE in the sample allowing one to evaluate molecular reorientational dynamics. Pulses with $\lambda_{ex} = 575$ nm are resonant with a two-photon transition of the 5CB molecules inducing an excited state grating. A large permanent dipole moment change of the 5CB molecules upon excitation induces reorganization of the solvent cage around the excited molecule. This solvent relaxation spectrally shifts the excited state–excited state transition which absorbs the probe beam. Therefore, the TG signal can follow the solvent reorganization dynamics. The solvent reorganization is observed to take place on a ps time scale, and is complete in 4 ps. In addition, at high intensities, absorption of a third photon populates a higher excited state which leads to fast vibrational radiationless relaxation, local heating, and the generation of an acoustic standing wave.

Electronic and nuclear OKE, excited state and acoustic wave gratings are all characterized by different symmetries of the nonlinear susceptibility $\chi^{(3)}$ tensor. This leads to distinct polarization characteristics in TG experiments for the various phenomena. We have demonstrated that one can suppress the TG signal from any given physical process by the right polarization selection, and in addition one can identify the origin of an unknown physical process by characterizing the polarization dependence of its TG signal.

It is possible to determine the $\chi^{(3)}$ symmetry of a process by, e.g., independent measurements of the signal intensities in a parallel and crossed grating configuration. However, with such an approach it is necessary to measure the absolute magnitude of two signals, which can only be related by

knowledge of the polarization characteristics of the entire optical detection setup. In the approach presented here, the $\chi^{(3)}$ symmetry can be deduced from a single number, the polarization angle β_0, which does not require the measurement of the absolute magnitude of the signals.

The method can be readily extended to the investigation of any physical process in an isotropic sample, allowing its identification and characterization. In principle, this approach can also be applied to anisotropic media. For anisotropic media, however, there will be more than the two independent elements of $\chi^{(3)}$ which are found for the isotropic samples [see Eqs. (4) and (5)]. The contribution of a particular effect to the signal will still depend on the polarization configuration. In general, however, it will not be possible to suppress the signal from one process completely. While this fact reduces, to a large extent, the power and elegance of the technique, the method may still be useful in the study of anisotropic media.

ACKNOWLEDGMENTS

The authors would like to thank S. R. Greenfield, V. J. Newell, and J. J. Stankus for technical assistance in the experiments. This work was supported by the National Science Foundation, Division of Material Research (DMR 87-18959). Additional suport was provided by the Office of Naval Research, Physics Division (N00014–89-J-1119). F. W. Deeg would like to thank the scientific committee of NATO for a postdoctoral fellowship administered through DAAD.

[1]H. J. Eichler, P. Guenter, and D. W. Pohl, *Laser-Induced Dynamic Gratings* (Springer, Berlin, 1986).
[2]M. D. Fayer, Annu. Rev. Phys. Chem. **33**, 63 (1982).
[3]IEEE J. Quantum Electron., Special Issue on Dynamic Gratings and Four-Wave Mixing, edited by H. J. Eichler (1986).
[4]H. J. Eichler, G. Salje, and H. Stahl, J. Appl. Phys. **44**, 5383 (1973).
[5]P. G. de Gennes, J. Phys. Lett. **38**, 1 (1997); M. Fermigier, E. Guyon, P. Jenffer, and L. Petit, Appl. Phys. Lett. **36**, 361 (1980).
[6]K. A. Nelson and M. D. Fayer, J. Chem. Phys. **72**, 5202 (1980); R. J. D. Miller, R. Casalegno, K. A. Nelson, and M. D. Fayer, Chem. Phys. **72**, 371 (1982).
[7]R. J. D. Miller, M. Pierre, and M. D. Fayer, J. Chem. Phys. **78**, 5138 (1983); J. R. Salcedo, A. E. Siegman, D. D. Dlott, and M. D. Fayer, Phys. Rev. Lett. **41**, 131 (1978).
[8]D. H. Auston, C. V. Shank, and P. Lefur, Phys. Rev. Lett. **35**, 1035 (1976); B. Sermage, H. J. Eichler, J. P. Heritage, R. J. Nelson, and N. K. Dutta, Appl. Phys. Lett. **42**, 259 (1983).
[9]G. Eyring and M. D. Fayer, J. Chem. Phys. **81**, 4314 (1984).
[10]Chr. Bräuchle and D. M. Burland, Angew. Chem. Int. Ed. Engl. **22**, 582 (1983).
[11]A. D. Buckingham, Proc. Phys. Soc. B **69**, 344 (1956).
[12]K. Sala and M. C. Richardson, Phys. Rev. A **12**, 1036 (1975).
[13]Y. X. Yan and K. A. Nelson, J. Chem. Phys. **87**, 6240 (1987).
[14]P. G. de Gennes, *The Physics of Liquid Crystals* (Oxford University, New York, 1974).
[15]F. W. Deeg and M. D. Fayer, Chem. Phys. Lett. (submitted); F. W. Deeg, V. J. Newell, S. R. Greenfield, J. J. Stankus, and M. D. Fayer, J. Chem. Phys. (in preparation).
[16]C. David and D. Baeyens-Volant, Mol. Cryst. Liq. Cryst. **59**, 181 (1980).
[17]W. Liptay, *In Excited States I*, edited by E. C. Lim (Academic, New York, 1974), p. 129.
[18]B. Bagchi, D. W. Oxtoby, and G. R. Fleming, Chem. Phys. **86**, 257 (1984).
[19]M. R. Topp, P. M. Rentzepis, and P. R. Jones, Chem. Phys. Lett. **9**, 1 (1971).
[20]S. G. Su and J. D. Simon, J. Chem. Phys. **89**, 908 (1988).
[21]J. Etchepare, G. Grillon, J. P. Chambaret, G. Harmoniaux, and A. Orszag, Opt. Commun. **63**, 329 (1987).
[22]V. J. Newell, F. W. Deeg, S. R. Greenfield, and M. D. Fayer, J. Opt. Soc. Am. B **6**, 257 (1989).
[23]Y. R. Shen, *The Principles of Nonlinear Optics* (Wiley, New York, 1984).
[24]P. N. Butcher, *Nonlinear Optical Phenomena Bulletin 200* (Engineering Experiment Station, Ohio State University, Columbus, Ohio, 1965).
[25]R. W. Hellwarth, Prog. Quant. Electr. **5**, 1 (1977).
[26]R. W. Hellwarth, A. Owyoung, and N. George, Phys. Rev. A **4**, 2342 (1971).
[27]A. B. Myers and R. M. Hochstrasser, IEEE J. Quantum Electron. **22**, 1482 (1986).
[28]L. Genberg, Q. Bao, S. Gracewski, and R. J. D. Miller, Chem. Phys. **131**, 81 (1989).
[29]F. W. Deeg, J. J. Stankus, S. R. Greenfield, V. J. Newell, and M. D. Fayer, J. Chem. Phys. **90**, 6893 (1989).